Nano Energy 131 (2024) 110204

Contents lists available at ScienceDirect

Nano Energy

journal homepage: www.elsevier.com/locate/nanoen

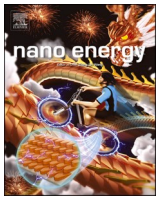

Suppressing non-radiative recombination and tuning morphology via central core asymmetric substitution for efficient organic solar cells

Xiaodong Si [a,1], Wendi Shi [a,1], Ruohan Wang [a], Wenkai Zhao [b], Zhaochen Suo [a], Zhen Fu [c], Guankui Long [b], Xiaotao Hao [c], Zhaoyang Yao [a], Xiangjian Wan [a,*], Chenxi Li [a,*], Yongsheng Chen [a,*]

[a] State Key Laboratory of Elemento-Organic Chemistry, Frontiers Science Center for New Organic Matter, The Centre of Nanoscale Science and Technology and Key Laboratory of Functional Polymer Materials, Institute of Polymer Chemistry, Renewable Energy Conversion and Storage Center (RECAST), Tianjin Key Laboratory of Functional Polymer Materials, Nankai University, Tianjin 300071, China
[b] School of Materials Science and Engineering, National Institute for Advanced Materials, Nankai University, Tianjin 300071, China
[c] School of Physics, State Key Laboratory of Crystal Materials, Shandong University, Jinan 250100, China

ARTICLE INFO

Keywords:
Organic solar cells
Non-fullerene acceptors
Energy loss
Morphology

ABSTRACT

It is necessary and challenging to achieve high-efficiency organic solar cells (OSCs) by suppressing nonradiative energy loss (ΔE_{nr}) and fine-tuning active layer morphology through the delicate active material design. In this study, we design two asymmetric acceptors, a-CH-ThCl and a-CH-Th2Cl, featuring asymmetric conjugated substitutions on central cores via single bond linkages. Single crystals analysis indicate that these two acceptors exhibit intense J-aggregation induced by the asymmetric substitution, which favours for their high photoluminescence quantum yields and contributes to reducing non-radiative recombination. Meanwhile, the two asymmetric acceptors demonstrate enhanced miscibility and optimized morphology with the donor D18. Consequently, the binary device based on D18: a-CH-Th2Cl demonstrates an impressive efficiency of up to 19.10 % with a high open-circuit voltage of 0.935 V, attributed to the remarkably low ΔE_{nr} of 0.179 eV and optimized morphology. These results provide an effective strategy for material design to optimize molecular packing, reduce non-radiative recombination and tune active layer morphology to achieve high-efficiency OSCs.

1. Introduction

In recent years, the photovoltaic performance of organic solar cells (OSCs) has substantially increased, mainly due to innovations in active layer materials, device engineering and a deeper understanding of device mechanisms [1–19]. In particular, the introduction of A-D-A type non-fullerene acceptors (NFAs) such as ITIC, Y6, and their derivatives has significantly boosted OSC efficiencies to impressive levels [20–22]. The efficiency of OSCs is primarily constrained by the large nonradiative energy loss (ΔE_{nr}) and unfavourable active layer morphology [23–29]. Achieving high-performance OSCs by suppressing ΔE_{nr} and fine-tuning the active layer morphology through delicate active material design remains a challenging task. Over the past decade, researchers have designed many acceptor materials, often introducing steric hindrance bulk groups to decrease the aggregation induced emission and thereby achieving low ΔE_{nr} [30–32]. However, the significant steric hindrance also impedes efficient molecular packing and aggregation, resulting in low charge mobilities, poor morphologies, and consequently inferior device performance [33–37]. Thus, it remains a challenge to regulate molecular packing through material design to minimize nonradiative recombination without compromising other critical properties such as charge mobility, active layer blend morphology, and more.

Considering the significant role of central core in the molecular packing and other optoelectronic properties for Y-series acceptors, both our group and others have designed a series of acceptors with extended conjugation central cores based on Y-series acceptors [36–44]. These designs have efficiently strengthened intermolecular interactions, facilitated carrier transport, and achieved impressive efficiencies. Specifically, the interaction between central cores and end groups significantly affects intermolecular packing as demonstrated by single crystal analysis results [36]. However, our recent results indicated that larger extension conjugation on the central core could prompt the formation of

* Corresponding authors.
E-mail addresses: xjwan@nankai.edu.cn (X. Wan), lichenxi@nankai.edu.cn (C. Li), yschen99@nankai.edu.cn (Y. Chen).
[1] These authors contributed equally.

https://doi.org/10.1016/j.nanoen.2024.110204
Received 13 July 2024; Received in revised form 15 August 2024; Accepted 2 September 2024
Available online 6 September 2024

excessively intense packing, unfavourable for suppressing the ΔE_{nr} and forming suitable morphology [45]. It prompt us to search for new method to design acceptors.

In this work, we report two new acceptors called a-CH-ThCl and a-CH-Th2Cl, featuring asymmetric substitutions on the central cores. Unlike the conventional asymmetric acceptor design strategies by modification of end groups, side chains and molecular backbones, the two asymmetric acceptors are designed by introducing chlorinated thiophene units on the central pyrazine cores via a single bond linkage (Fig. 1). Herein, single bond linkages can maintain conjugation between grafted thiophene units and pyrazine. It should be noted that the C-C linkage strategy has been demonstrated by Dong and coworkers in organic semiconductor materials designed for organic light-emitting transistors, which exhibited high mobility and strong emission due to efficiently extended π conjugation and compact J-aggregation packing in the solid state [46]. Using the unconventional asymmetric design strategy, the two acceptors showed compact J-aggregation verified in their single crystals and demonstrated high emission and low non-radiative recombination. Meanwhile, the two asymmetric acceptors demonstrate enhanced miscibility and optimized morphology with the donor D18. Consequently, the a-CH-Th2Cl based device demonstrated a remarkable PCE up to 19.10 % with a low ΔE_{nr} of 0.179 eV, among the best result reported to date for asymmetric acceptor-based binary OSCs. These results demonstrate that central core asymmetric substitution via the single bond linkage is an effective approach to regulate molecular packing, effectively reducing ΔE_{nr} and finely tuning the blend film morphology to obtain efficient OSCs.

2. Result and discussion

2.1. Material properties

The chemical structures of CH-ThCl, a-CH-ThCl, and a-CH-Th2Cl are shown in Fig. 1b. The synthetic procedures of a-CH-ThCl and a-CH-Th2Cl followed a similar method as we have previously reported [41], and the detailed procedures and characterizations are provided in the Supporting Information (SI). The influence of central core asymmetric on the molecular geometry was firstly studied by density functional theory (DFT) calculations. As illustrated in Figure S1a, similar to the symmetric acceptor CH-ThCl, the two asymmetric molecules both displayed a relatively planar geometry. Particularly, the thiophene units linked on the central cores are nearly in the same plane with the pyrazine central core units, with the dihedral angles 0.19° and 0.23°, respectively. As shown in Figure S1b, with the asymmetric central substitutions, a-CH-ThCl and a-CH-Th2Cl showed improved dipole moments and different electrostatic potential (ESP) distributions compared to the symmetric molecule CH-ThCl, which will have an influence on their packing behaviors and interactions with donor materials. To explore the effect of ESP difference on the intermolecular interaction between donor and acceptor, we employ the program Multiwfn to

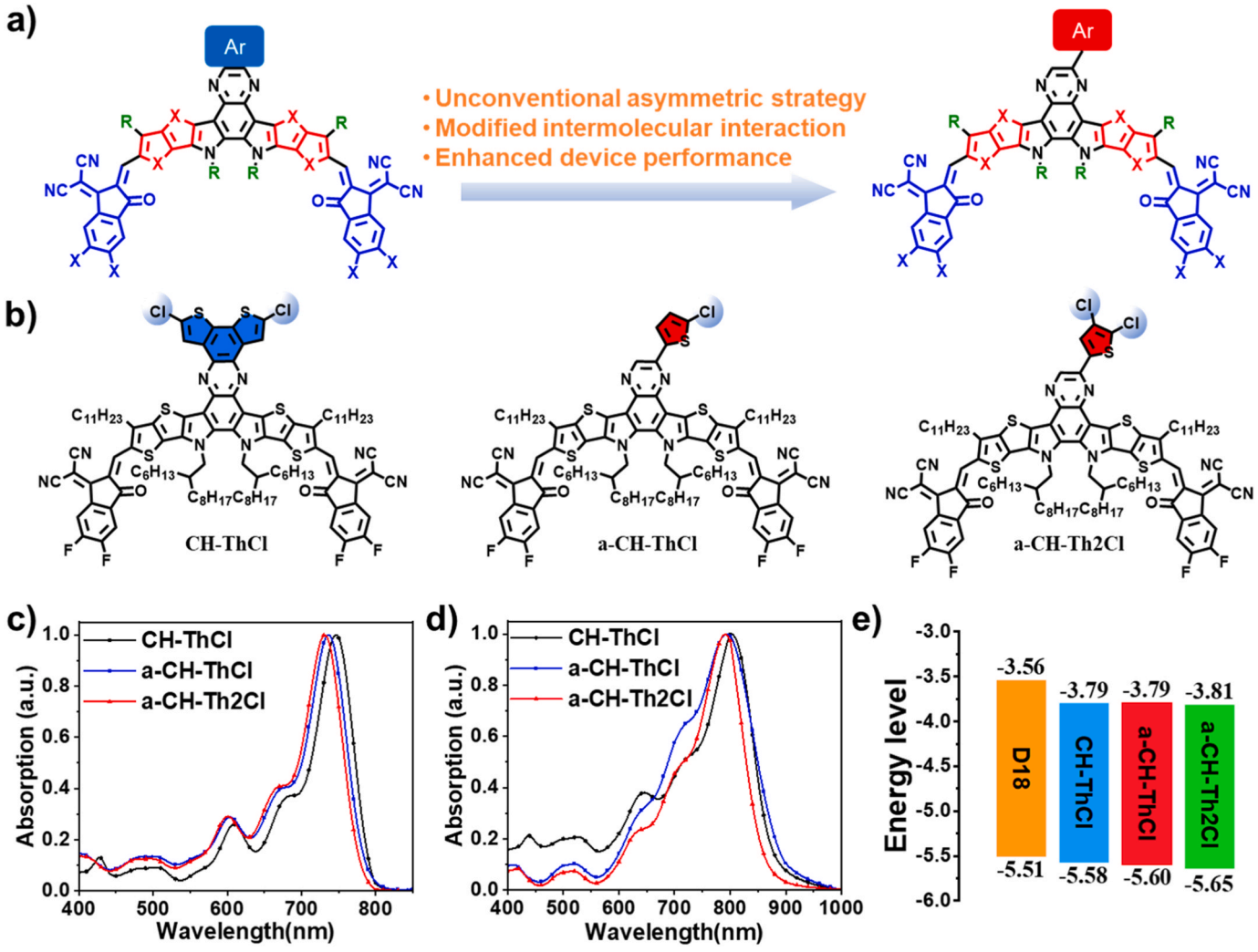

Fig. 1. a) Illustration of the design strategy. b) Chemical structure of CH-ThCl, a-CH-ThCl and a-CH-Th2Cl. c, d) The absorption spectra of CH-ThCl, a-CH-ThCl and a-CH-Th2Cl in solution and films. e) Energy level diagram of D18, CH-ThCl, a-CH-ThCl and a-CH-Th2Cl.

conduct quantitative analysis based on ESP. As shown in Table S1, compared to CH-ThCl, the slightly larger ν values of the two asymmetric acceptors are closer to 0.25, which indicated a stronger ESP-induced intermolecular interaction with the donor polymer[47]. Moreover, asymmetric acceptors have lower σ^2_{tot} than that of CH-ThCl, indicating that the two asymmetric acceptors and D18 tend to form more suitable phase separation with the interpenetrating network structures [48].

The UV/vis absorption spectra of CH-ThCl, a-CH-ThCl and a-CH-Th2Cl in dilute chloroform (CF) solution and film states are depicted in Figs. 1c and 1d. In CF solution, CH-ThCl, a-CH-ThCl, and a-CH-Th2Cl exhibited maximum absorption (λ_{max}) peaks at 746, 736 and 731 nm, respectively. In film states, their absorptions were all red-shifted with λ_{max} peaks at 801, 793 and 791 nm, respectively. This red-shift suggests the presence of strong intermolecular interactions in the solid films. Compared to CH-ThCl, the slight blue-shifted absorptions of a-CH-ThCl and a-CH-Th2Cl are caused by the reduced intramolecular charge transfer effect due to the unfused asymmetric central units. The energy levels of D18, CH-ThCl, a-CH-ThCl and a-CH-Th2Cl were estimated using electrochemical cyclic voltammetry (CV). From the CV curves (Figure S2-4), the lowest unoccupied molecular orbital (LUMO) and highest occupied molecular orbital (HOMO) levels of D18, CH-ThCl, a-CH-ThCl, and a-CH-Th2Cl were estimated to be −3.56/-5.51, −3.79/-5.58, −3.79/-5.60, and −3.81/-5.65 eV, respectively, indicating that the asymmetric central core substitutions have little effect on the LUMO levels, only slightly affect the HOMO levels since the LUMO/HOMO levels of A-D-A architecture molecules are primarily determined by the end groups and molecular backbones, respectively [21].

2.2. Single crystal analysis

To further elucidate the impact of the asymmetric central core on acceptor geometry and intermolecular interactions, we cultivate crystals of the three acceptors. The crystals of three crystals were successfully obtained in chloroform by solvent diffusion with methanol as the poor solvent. As depicted in Fig. 2a, all the three acceptors display similar banana-shaped molecular geometries and planar-lock skeletons due to strong intramolecular S···O interactions. a-CH-ThCl and a-CH-Th2Cl exhibit slightly larger π-core torsions with dihedral angles of 7.52° and 9.88°, respectively, compared to that of CH-ThCl (2.38°). Additionally, the grafted thiophene units on the central cores of a-CH-ThCl and a-CH-Th2Cl align nearly in the same plane with the adjacent pyrazine unit with the dihedral angles of 6.92° and 8.11°, respectively, indicating that the asymmetric design on the central units has little effect on the overall planarity of the two asymmetric acceptors but provide alternative channels for subtle tuning the molecular packing modes.

As depicted in Fig. 2b, unlike Y6 crystal, the three single crystals display two-dimensional arrangements through multiple intermolecular π-π interactions. All of them feature three types of intense π-π interactions, namely, end group to end group mode (E/E), and two types of the end group to the central core mode (dual E/C-1 and dual E/C-2). Particularly, mode 1 and mode 3 show the slip-stacked J-Aggregation behaviours. In details, a-CH-ThCl and a-CH-Th2Cl crystals show relatively smaller E/E π–π distance with values ca. 3.303/3.336 Å than that CH-ThCl with value of 3.366 Å, indicating stronger π–π stackings between two terminal units for the two asymmetric acceptors. Moreover, the dual E/C-1 and dual E/C-2 modes also exhibit strong π-π interactions for CH-ThCl, a-CH-ThCl and a-CH-Th2Cl with distances of 3.430/3.435/3.542 Å for Mode 2 and 3.416/3.313/3.435 Å for Mode 3, respectively.

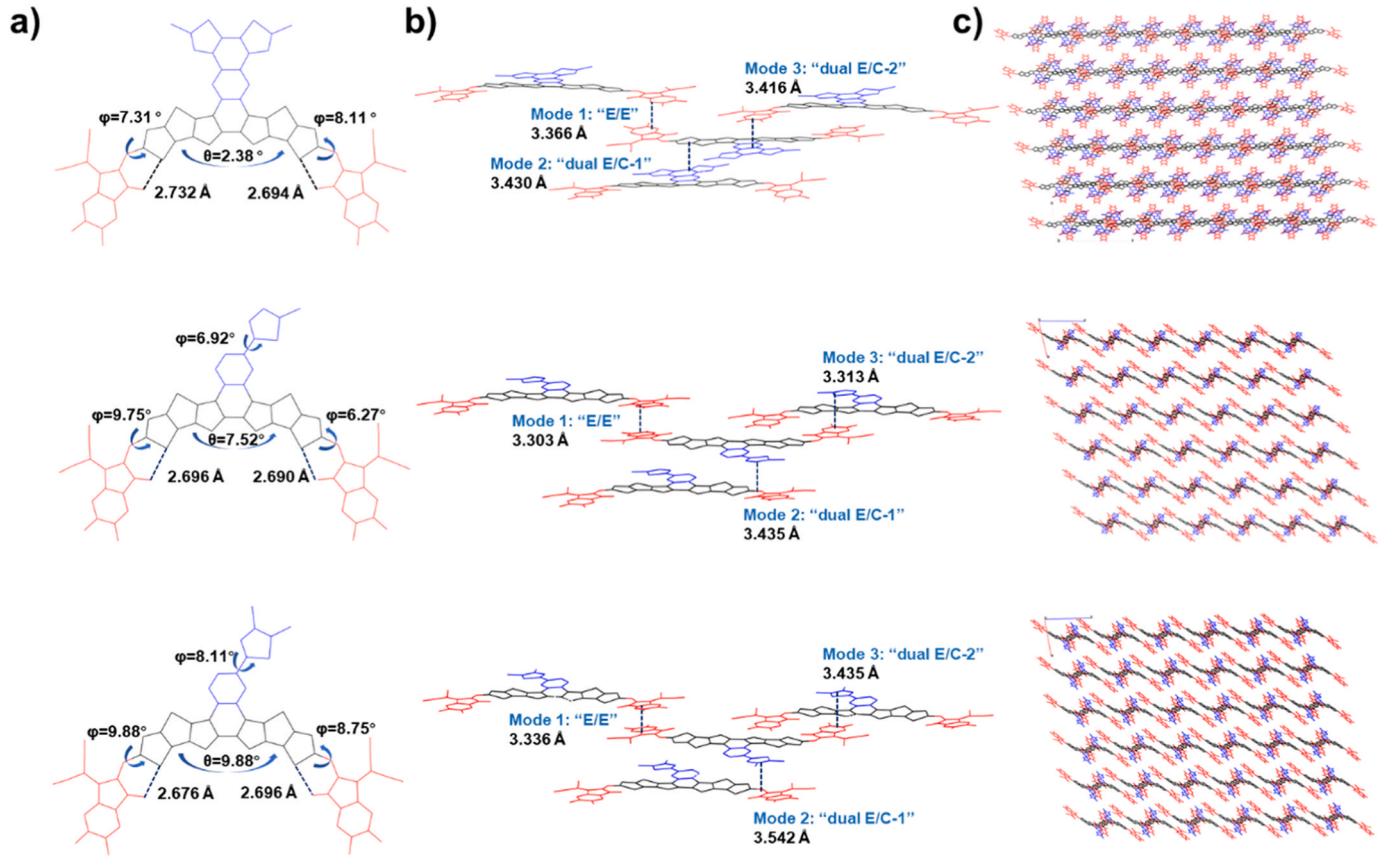

Fig. 2. a) The single-molecule view of single-crystal structures. b) The intermolecular packing modes in the single crystal of CH-ThCl, a-CH-ThCl and a-CH-Th2Cl. c) Molecular packing patterns in CH-ThCl, a-CH-ThCl and a-CH-Th2Cl single-crystals. The intramolecular S…O distances, the π-core torsions angles (θ), the D-A and thiophene-central core dihedral angles (φ) were given. Alkyl chains and H atoms are hidden for clarity.

The electron transfer integral (V_E), and hole transfer integral (V_H) of CH-ThCl, a-CH-ThCl and a-CH-Th2Cl were calculated (Table S2-4) to evaluate the charge transfer property [41,49]. The "E/E" molecular packing (Mode 1) in a-CH-Th2Cl possessed the largest V_E and V_H with values of 54.78 and 65.80 meV, respectively, among the three molecules, indicating the asymmetric central core unit can effectively tune and improve the charge transport in films. As shown in Fig. 2c, the three molecules present 2D packing modes. The molecular packing densities of the three molecules were estimated. As listed in Table S5, a-CH-Th2Cl shows the molecular packing density of 62.3 %, larger than that of CH-ThCl and a-CH-ThCl (60.1 % and 56.8 %). These results demonstrate that introducing the central core asymmetric substitution via a single bond linkage can provide efficient venues to subtle manipulate and tune the molecular planarity, intermolecular crystal packing and charge transport channels in the solid states.

2.3. Photovoltaic performance

To evaluate the photovoltaic performance of CH-ThCl, a-CH-ThCl and a-CH-Th2Cl, binary OSCs with a conventional structure of ITO/PEDOT: PSS/Active layer/PNDIT-F3N/Ag (Fig. 3a) were fabricated, in which D18 was selected as donor polymer owing to the matched absorption and energy levels with the three acceptors. The detailed device fabrication procedures and conditions are provided in Table S6-8. The optimized photovoltaic parameters of the three devices are listed in Table 1, and the corresponding current density-voltage (*J-V*) curves are depicted in Fig. 3b. As listed in Table 1, the device based on a-CH-ThCl exhibited a PCE of 17.83 %, which is slightly higher than that of CH-ThCl based device with efficiency of 17.68 %. Impressively, a PCE of 19.10 % is achieved for a-CH-Th2Cl based device due to the enhanced J_{sc} and FF compared to CH-ThCl and a-CH-ThCl based devices. The external quantum efficiency (EQE) curves of the optimized devices are shown in Fig. 3c. The three devices, particularly a-CH-Th2Cl based device, demonstrated high photon responses across the light absorption ranges. The calculated J_{sc} values from the EQE curves align well with those measured in the *J-V* curves.

Table 1
Photovoltaic parameters of the optimized devices.

Active layer	V_{oc}(V)	J_{sc}(mA cm^{-2})	$J_{sc}^{(a)}$(mA cm^{-2})	FF(%)	PCE(%)
D18: CH-ThCl	0.939	25.05	23.98	75.11	17.68
D18: a-CH-ThCl	0.934	25.27	24.02	75.47	17.83
D18: a-CH-Th2Cl	0.935	26.18	25.19	78.01	19.10

[(a)] Current densities calculated from EQE data.

2.4. Energy loss analysis

To study the influence of asymmetric central unit on energy loss (E_{loss}), we conducted the energy loss analysis. As listed in Table 2, the three acceptors-based devices all showed small total E_{loss} with values around 0.5 eV. Particularly, the a-CH-ThCl based device showed the lowest value of 0.492 eV compared to that of CH-ThCl (0.495 eV) and a-CH-Th2Cl (0.509 eV) based devices. The detailed E_{loss} components for the three devices were investigated following the established methods. As listed in Table 2, the three devices showed the nearly same ΔE_1 around 0.27 eV and very small ΔE_2 below 0.1 eV. The ΔE_3, also called nonradiative energy loss, is the determined energy loss in OSCs. It was calculated using two different methods and showed a similar trend and impressively small values below 0.2 eV for the three acceptors based devices. As illustrated in Fig. 3e, the a-CH-ThCl and a-CH-Th2Cl based devices showed EQE_{EL} of 11.6 E^{-4} and 9.9 E^{-4}, respectively, higher than that of CH-ThCl. Impressively low ΔE_3 with values of 0.175 and 0.179 eV were afforded for the a-CH-ThCl and a-CH-Th2Cl based devices, respectively, according to the equation of $\Delta E_3 = -kTln(EQE_{EL})$, smaller than that of the CH-ThCl based device with a value of 0.185 eV. To our knowledge, it is among the lowest ΔE_3 values for devices with efficiencies over 19 % (Fig. 3f, details in Table S9). As reported by Gao et al., the photoluminescence efficiencies of the pristine material components define the limit of ΔE_3 in OSCs [50]. To explain the low ΔE_3 values of the three devices, the photoluminescence quantum yield (PLQY) of CH-ThCl, a-CH-ThCl and a-CH-Th2Cl were measured. As shown in Figure S5, the films of a-CH-ThCl and a-CH-Th2Cl demonstrate PLQY of 5.62 % and 5.54 %, respectively, higher than that of CH-ThCl with the value of 5.49 % under the same measured conditions. The high PLQY of the two asymmetric acceptors might originate from

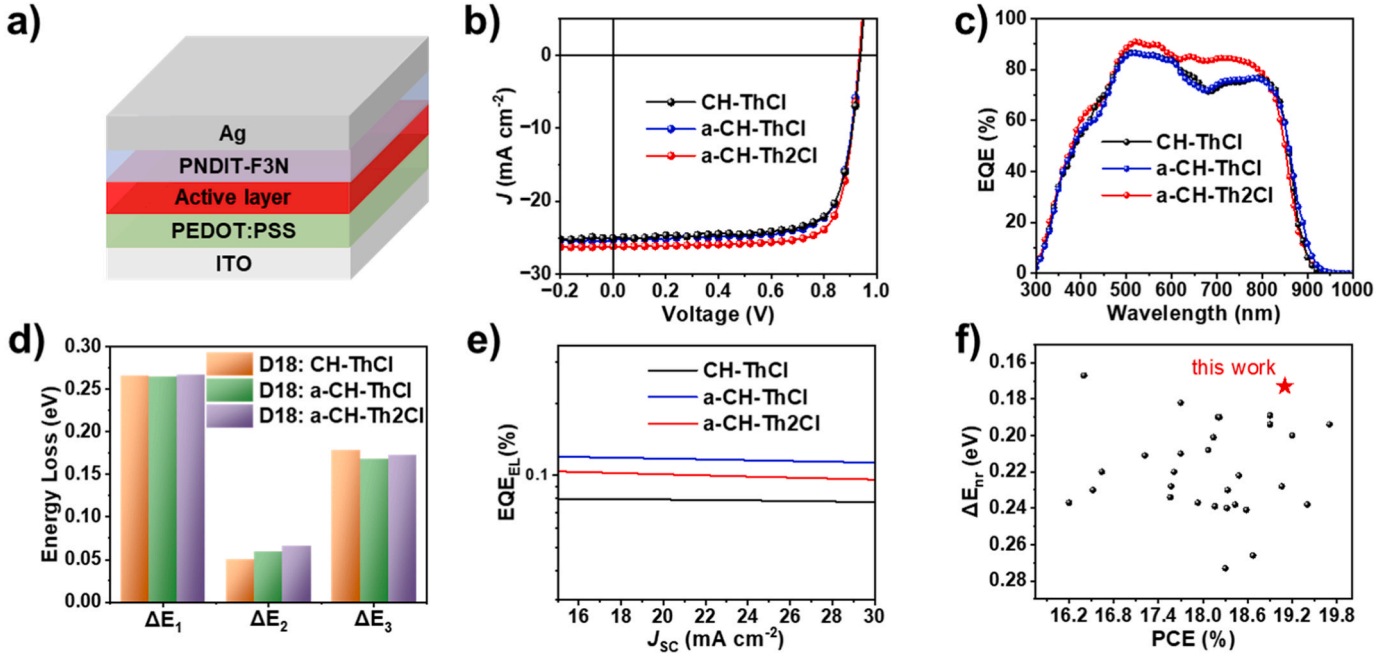

Fig. 3. a) Architecture of the OSC device. b, c) J-V and EQE curve for the optimized devices. d, e) E_{loss} diagram and EQE_{EL} spectra for the optimized devices. f) Plot of ΔE_3 vs PCEs for reported OSCs.

Table 2
Energy loss analysis of the devices.

Active layer	V_{oc} (V)	$E_g^{(a)}$ (eV)	E_{loss} (V)	$V_{oc,\ sq}^{(b)}$ (V)	$\Delta E_1^{(c)}$ (eV)	$V_{oc,\ rad}^{(d)}$ (V)	ΔE_2 (eV)	$\Delta E_3^{(1)}$ (cal.V)	EQE_{EL} (%)	$\Delta E_3^{(2)}$ (exp.V)
D18: CH-ThCl	0.939	1.434	0.495	1.168	0.266	1.118	0.050	0.179	0.079	0.185
D18: a-CH-ThCl	0.934	1.426	0.492	1.161	0.265	1.102	0.059	0.168	0.116	0.175
D18: a-CH-Th2Cl	0.935	1.444	0.509	1.177	0.267	1.111	0.066	0.173	0.099	0.179

(a) E_g was estimated via EQE spectra of the devices.
(b) $V_{oc,\ sq}$ is calculated according to the SQ limit.
(c) $\Delta E_1 = E_g - V_{oc,\ sq}$.
(d) $V_{oc,\ rad}$ is the V_{oc} when there is only radiative recombination and are calculated from EL and sEQE measurements. ΔE_3 ($\Delta E_3 = q\Delta V_{nr}$) is determined by two approaches: 1) calculated by q ($V_{oc,\ rad}$ -V_{oc}) and 2) obtained from the equation $q\Delta V_{nr} = -kT\ln EQE_{EL}$ by measuring the device EQE_{EL}.

enhanced J-aggregations in the solid films as shown in the single crystal packings according to the established results [51].

2.5. Exciton and charge dynamics analysis

Femtosecond transient absorption spectroscopy was used to study the exciton dynamics (Fig. 4a-c) [52]. The hole-transfer behavior of the three blend films were investigated by selective photoexcitation of the acceptors at a wavelength of 800 nm. Ground state bleach (GSB) peaks with negative signals at ~710 nm corresponded to acceptors are observed. With the decrease of acceptors bleach peak (≈710 nm) in the first 100 ps, the GSB bleach peak of D18 (≈590 nm) emerged in the TA spectra of three blend films (Fig. 4a-c and Figure S6a-c). Since there was no signal at ≈590 nm in the photo excited acceptors neat film (Figure S7), the GSB kinetics at ≈590 nm were used to represent the hole-transfer kinetics of the blend films. The exciton dissociation

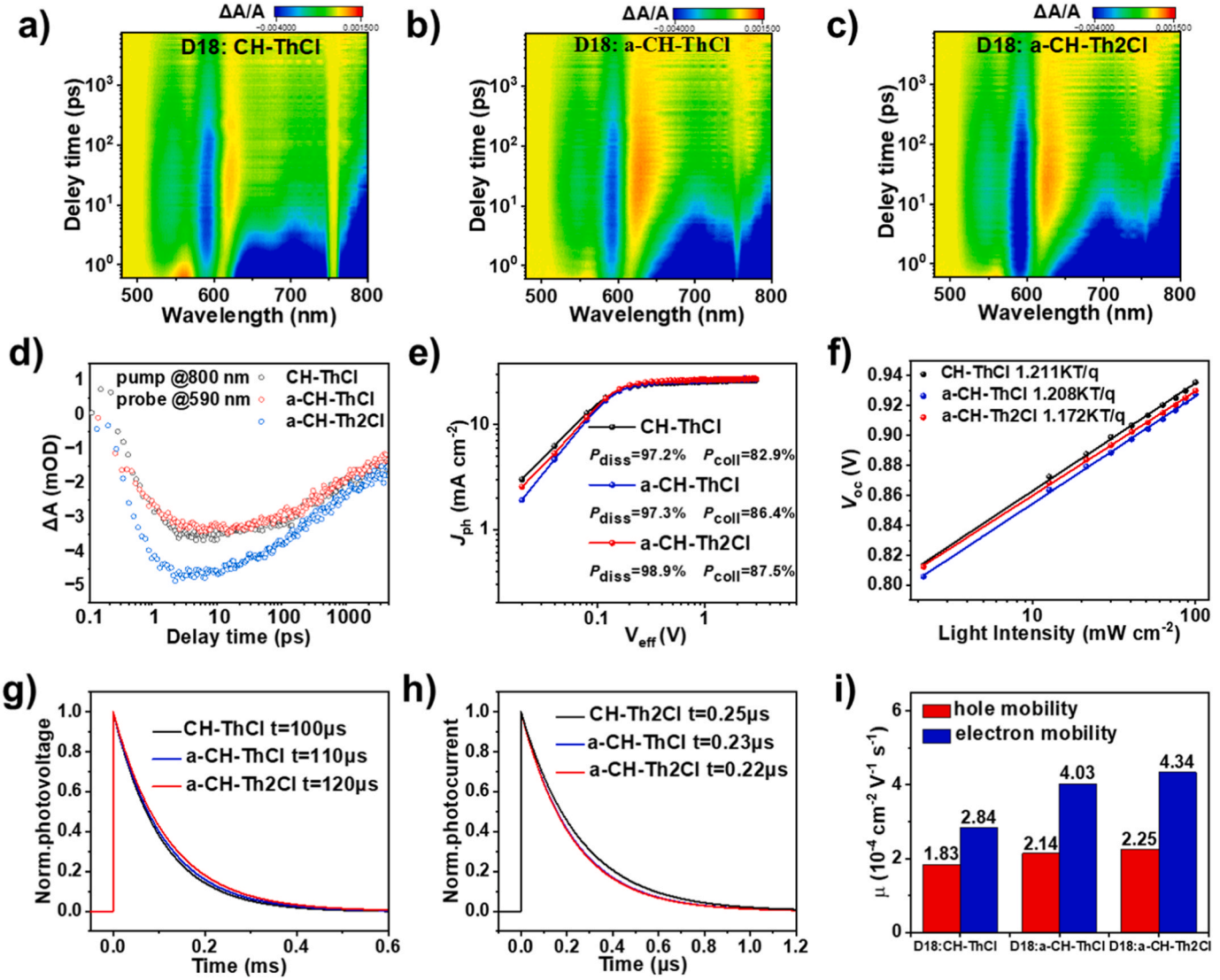

Fig. 4. a-c) 2D color plots of TA spectra of D18: CH-ThCl, D18: a-CH-ThCl, and, D18: a-CH-Th2Cl films. d) The kinetics curves of GSB (590 nm) for donor. e) J_{ph} versus V_{eff} curves of CH-ThCl, a-CH-ThCl and a-CH-Th2Cl based devices. f) V_{oc} versus light intensity of the optimized devices. g, h) TPV and TPC measurements of the optimized devices. i) The carrier transport properties of the optimized devices.

dynamics were investigated by fitting the GSB data at 590 nm using a double exponential function to get two important parameters τ1 and τ2 (Fig. 4d), which refer to the time scale of ultrafast exciton dissociation at the donor–acceptor interface and the slow diffusion of excitons toward the interface before dissociation, respectively [53]. The τ1 values for CH-ThCl, a-CH-ThCl and a-CH-Th2Cl based blend films with D18 are 831, 751 and 436 fs, respectively. The τ2 values are fitted to be 16.52, 14.85 and 10.01 ps for D18: CH-ThCl, D18: a-CH-ThCl and D18: a-CH-Th2Cl blends, respectively. The relatively small τ1 and τ2 for the D18: a-CH-Th2Cl blends indicate that exciton dissociation and diffusion are more efficient, which is benificial to suppress the charge recombination, thus improve the J_{sc} and FF [54,55]. The dependence of photocurrent density (J_{ph}) on effective voltage (V_{eff}) was used to explore the exciton dissociation and charge collection properties of the three devices (Fig. 4e). The values of J_{ph}/J_{sat} under short-circuit conditions/maximum power output conditions were 97.2 % /82.9 %, 97.3 %/ 86.4 % and 98.9 %/ 87.5 % for the CH-ThCl, a-CH-ThCl and a-CH-Th2Cl based devices, respectively, indicating that the a-CH-Th2Cl based device exhibited the highest charge dissociation and collection efficiencies. Furthermore, to investigate the charge recombination behavior in the three devices, the light intensity (P) dependence of J_{sc} and V_{oc} were measured. As shown in Figure S8, the J_{sc} showed the linear correlations with Plight with α values over 0.99, indicating the less bimolecular charge recombination in the three devices. Additionally, the trap-assisted recombination were investigated from the plotting of the V_{oc} versus light intensity. The a-CH-Th2Cl devices showed the smallest slope with value of 1.172 kT/q, suggesting a reduced occurrence of trap-assisted recombination (Fig. 4f). Transient photocurrent (TPC) and transient photovoltage (TPV) measurements were used to further investigate the charge extraction and recombination properties for the three acceptors based devices. As depicted in Fig. 4g-h, the two asymmetric acceptors based devices exhibited longer carrier lifetime and shorter charge extraction time than the symmetric acceptor CH-ThCl based device. The space-charge-limited current (SCLC) method was employed to measure the charge mobilities of the three blend films. As illustrated in Fig. 4i, the blend film of D18: a-CH-Th2Cl and D18: a-CH-ThCl exhibited higher electron/hole mobilities with values of $4.34\times10^{-4}/2.25\times10^{-4}$ cm^{-2} V^{-1} s^{-1} and $4.03\times10^{-4}/2.14\times10^{-4}$ cm^{-2} V^{-1} s^{-1}, respectively, compared to the D18:CH-ThCl blend film, which had values of $2.84\times10^{-4}/1.83\times10^{-4}$ cm^{-2} V^{-1} s^{-1}.

2.6. Morphology analysis

As discussed above, the two asymmetric acceptors-based devices showed efficient processes of hole transfer, exciton dissociation and charge collection, and thus enhanced J_{sc} and FF, which are primarily attributed to their active layer morphologies. Atomic force microscopy (AFM) was used to study the surface morphologies of the three blend films. As depicted in Figs. 5a and 5b, the three blend films all showed uniform and smooth surfaces. In particular, the a-CH-Th2Cl blend film displayed more smoother surface morphology with a root-mean-square roughness (Rq) value 0.94 nm compared to other two blend films. AFM-based infrared spectroscopy (AFM-IR) was conducted to probe the fibril structures of the three blend films, using the specific infrared (IR) absorption at 2215 cm^{-1} for the three acceptors (Figure S9). As shown in Fig. 5b, the CH-ThCl, a-CH-ThCl and a-CH-Th2Cl based blend films

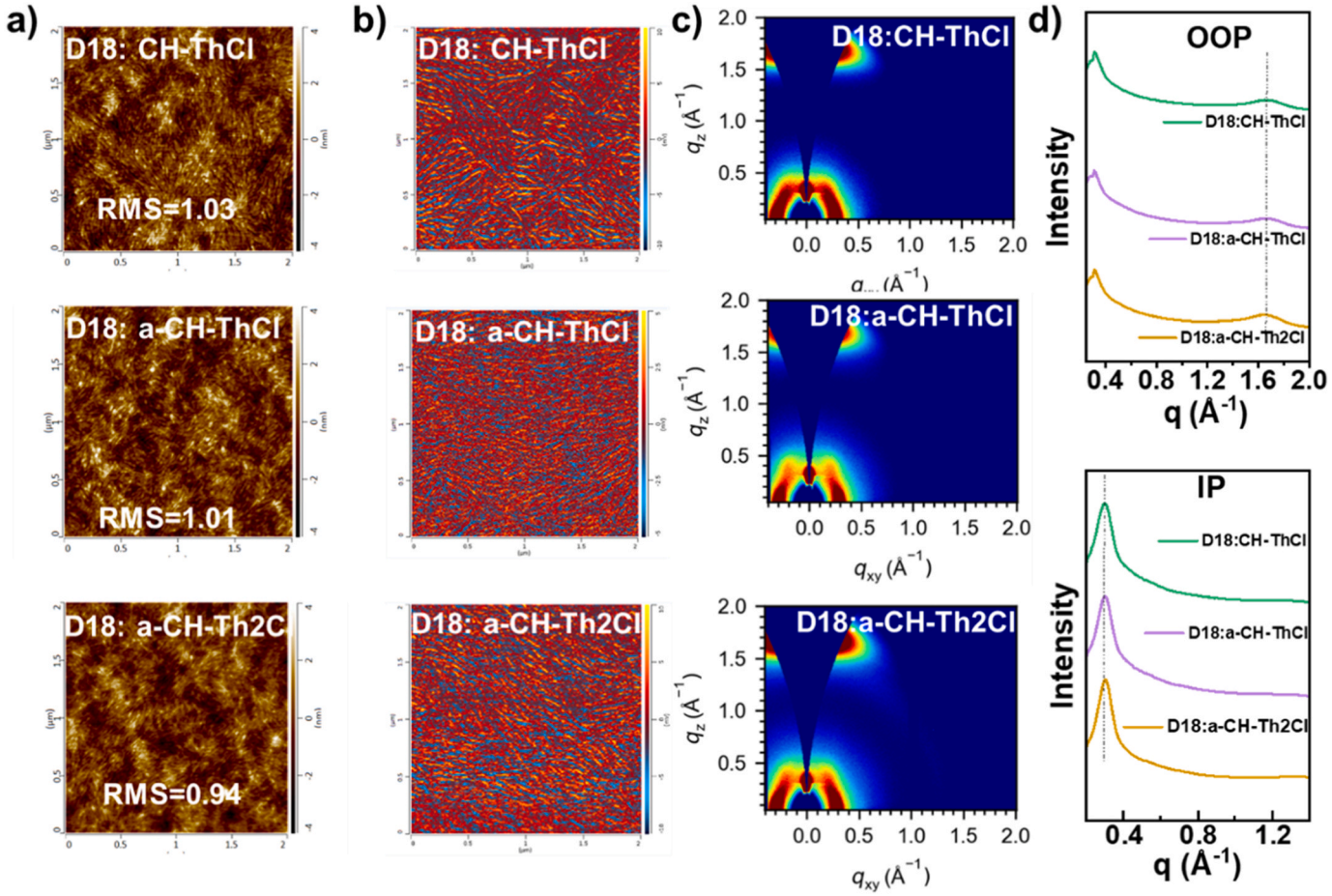

Fig. 5. a) AFM height and b) AFM-IR images recorded at 2215 cm-1 of the blend films. c) 2D GIWAXS patterns of optimized blend films. d) The corresponding out-of-plane (OOP) and in-plane (IP) extracted line-cut profiles of blend films.

showed distinct fibrillar network interpenetrating structures with the statistic diameters of 12.3, 11.6 and 10.2 nm, respectively (Figure S10). The small roughness and statistic diameter of the a-CH-Th2Cl blend film can facilitate the charge transport and suppress the carrier recombination. The contact angles of water and ethylene glycol droplets on the surfaces of various films were measured to determine the surface tensions of the three acceptors (Figure S11) and their Flory-Huggins interaction values (χ) with donor polymer D18. As listed in Table S10, the surface tensions for CH-ThCl, a-CH-ThCl, and a-CH-Th2Cl were 26.2, 25.9, and 25.8 mN m^{-1}, respectively. Compared to D18: CH-ThCl with a χ value of 0.48, D18: a-CH-ThCl and D18: a-CH-ThCl showed lower χ with values of 0.44 and 0.43, respectively, indicating better miscibility for the two asymmetric acceptors with D18 and attributed to the smoother surface with reduced nanofiber in the a-CH-ThCl and a-CH-Th2Cl blend films with D18.

Grazing incidence wide-angle X-ray scattering (GIWAXS) was employed to investigate the detailed molecular stacking information for the three acceptors and their blend films with donor D18. As shown in Figure S12, in the neat films, the three acceptors all adopted a face-on packing with the clear (010) peaks in the out-of-plane (OOP) direction and (100) peaks in the in-plane (IP) direction. The π-π stacking distances of CH-ThCl, a-CH-ThCl and a-CH-Th2Cl are 3.75, 3.76, and 3.79 Å, respectively. The corresponding crystal coherence lengths (CCLs) are 20.34, 20.05 and 20.41 Å, respectively. As shown in Fig. 5c-d, the three acceptors blend films also showed predominant face-on molecular stacking with clear (010) peaks in OOP direction and (100) peaks in IP direction. From the (010) peaks in the OOP directions, the three blend films aslo showed the similar π-π stacking distances and CCL are 3.75/ 22.44, 3.81/22.53, and 3.81/ 22.70 Å, respectively. Clearly, the two asymmetric acceptors in neat and blend films all exhibited nearly the same π-π packing distances and CCL compared with those of CH-ThCl (Table S11), indicating that the asymmetric central core units, despite with reduced conjugation, have no negative effect but can subtlety tune the homo and hetero intermolecular interactions in their blend films.

3. Conclusions

In summary, we have designed and synthesized two acceptor molecules a-CH-ThCl and a-CH-Th2Cl, featuring asymmetric central core units via the single bond linkage. The asymmetric central core can subtly tune the molecular packing and intermolecular interaction, and provide a delicate balance between crystallinity and the miscibility with the donor. Thus, the asymmetric acceptor a-CH-Th2Cl based devices showed an impressive efficiency of 19.10 %, with a low non-radiative energy loss of 0.179 eV, among the best results reported to date for asymmetric acceptor based binary OSCs. Our results underscore the significant role of central core asymmetric substitution in Y-series acceptors and present an effective strategy for reducing non-radiative recombination and tuning active layer morphology to achieve high-efficiency OSCs.

CRediT authorship contribution statement

Wendi Shi: Investigation. **Xiaodong si:** Investigation. **Yongsheng Chen:** Supervision. **Wenkai Zhao:** Investigation. **Ruohan Wang:** Investigation. **Zhen Fu:** Investigation. **Zhaochen Suo:** Investigation. **Xiaotao Hao:** Investigation. **Guankui Long:** Investigation. **Zhaoyang Yao:** Investigation. **Chenxi Li:** Supervision. **Xiangjian Wan:** Supervision, Conceptualization.

Declaration of Competing Interest

The authors declare that they have no known competing financial interests or personal relationships that could have appeared to influence the work reported in this paper.

Data Availability

Data will be made available on request.

Acknowledgements

The authors gratefully acknowledge the financial support from Ministry of Science and Technology of the People's Republic of China (National Key Research and Development Program of China, 2022YFB4200400, 2019YFA0705900, 2023YFE0210400, 2022YFA1203304). National Natural Science Foundation of China (52025033, 52373189, 21935007, 22361132530).

Appendix A. Supporting information

Supplementary data associated with this article can be found in the online version at doi:10.1016/j.nanoen.2024.110204.

References

[1] A.J. Heeger, 25th anniversary article: bulk heterojunction solar cells: understanding the mechanism of operation, Adv. Mater. 26 (2014) 10–28, https://doi.org/10.1002/adma.201304373.
[2] P. Bi, J. Wang, Y. Cui, J. Zhang, T. Zhang, Z. Chen, J. Qiao, J. Dai, S. Zhang, X. Hao, Z. Wei, J. Hou, Enhancing photon utilization efficiency for high-performance organic photovoltaic cells via regulating phase-transition kinetics, Adv. Mater. 35 (2023) 2210865, https://doi.org/10.1002/adma.202210865.
[3] T. Chen, S. Li, Y. Li, Z. Chen, H. Wu, Y. Lin, Y. Gao, M. Wang, G. Ding, J. Min, Z. Ma, H. Zhu, L. Zuo, H. Chen, Compromising charge generation and recombination of organic photovoltaics with mixed diluent strategy for certified 19.4% efficiency, Adv. Mater. 35 (2023) 2300400, https://doi.org/10.1002/adma.202300400.
[4] C. He, Y. Pan, Y. Ouyang, Q. Shen, Y. Gao, K. Yan, J. Fang, Y. Chen, C.-Q. Ma, J. Min, C. Zhang, L. Zuo, H. Chen, Manipulating the D: a interfacial energetics and intermolecular packing for 19.2% efficiency organic photovoltaics, Energy Environ. Sci. 15 (2022) 2537–2544, https://doi.org/10.1039/D2EE00595F.
[5] J.D. Servaites, M.A. Ratner, T.J. Marks, Organic solar cells: a new look at traditional models, Energy Environ. Sci. 4 (2011) 4410–4422, https://doi.org/10.1039/C1EE01663F.
[6] J. Hou, O. Inganäs, R.H. Friend, F. Gao, Organic solar cells based on non-fullerene acceptors, Nat. Mater. 17 (2018) 119–128, https://doi.org/10.1038/nmat5063.
[7] K. Jiang, J. Zhang, C. Zhong, F.R. Lin, F. Qi, Q. Li, Z. Peng, W. Kaminsky, S.-H. Jang, J. Yu, X. Deng, H. Hu, D. Shen, F. Gao, H. Ade, M. Xiao, C. Zhang, A.K. Y. Jen, Suppressed recombination loss in organic photovoltaics adopting a planar–mixed heterojunction architecture, Nat. Energy 7 (2022) 1076–1086, https://doi.org/10.1038/s41560-022-01138-y.
[8] J. Roncali, Molecular bulk heterojunctions: an emerging approach to organic solar cells, Acc. Chem. Res. 42 (2009) 1719–1730, https://doi.org/10.1021/ar900041b.
[9] A. Wadsworth, M. Moser, A. Marks, M.S. Little, N. Gasparini, C.J. Brabec, D. Baran, I. McCulloch, Critical review of the molecular design progress in non-fullerene electron acceptors towards commercially viable organic solar cells, Chem. Soc. Rev. 48 (2019) 1596–1625, https://doi.org/10.1039/C7CS00892A.
[10] L. Zhan, S. Li, X. Xia, Y. Li, X. Lu, L. Zuo, M. Shi, H. Chen, Layer-by-layer processed ternary organic photovoltaics with efficiency over 18%, Adv. Mater. 33 (2021) 2007231 https://doi.org/10.1002/adma.202007231.
[11] G. Zhang, J. Zhao, P.C.Y. Chow, K. Jiang, J. Zhang, Z. Zhu, J. Zhang, F. Huang, H. Yan, Nonfullerene acceptor molecules for bulk heterojunction organic solar cells, Chem. Rev. 118 (2018) 3447–3507, https://doi.org/10.1021/acs.chemrev.7b00535.
[12] L. Zhu, M. Zhang, J. Xu, C. Li, J. Yan, G. Zhou, W. Zhong, T. Hao, J. Song, X. Xue, Z. Zhou, R. Zeng, H. Zhu, C.-C. Chen, R.C.I. MacKenzie, Y. Zou, J. Nelson, Y. Zhang, Y. Sun, F. Liu, Single-junction organic solar cells with over 19% efficiency enabled by a refined double-fibril network morphology, Nat. Mater. 21 (2022) 656–663, https://doi.org/10.1038/s41563-022-01244-y.
[13] A. Devižis, J. De Jonghe-Risse, R. Hany, F. Nüesch, S. Jenatsch, V. Gulbinas, J.-E. Moser, Dissociation of charge transfer states and carrier separation in bilayer organic solar cells: a time-resolved electroabsorption spectroscopy study, J. Am. Chem. Soc. 137 (2015) 8192–8198, https://doi.org/10.1021/jacs.5b03682.
[14] L. Zuo, S.B. Jo, Y. Li, Y. Meng, R.J. Stoddard, Y. Liu, F. Lin, X. Shi, F. Liu, H. W. Hillhouse, D.S. Ginger, H. Chen, A.K.Y. Jen, Dilution effect for highly efficient multiple-component organic solar cells, Nat. Nanotechnol. 17 (2022) 53–60, https://doi.org/10.1038/s41565-021-01011-1.
[15] H. Lu, D. Li, W. Liu, G. Ran, H. Wu, N. Wei, Z. Tang, Y. Liu, W. Zhang, Z. Bo, Designing A-D-A type fused-ring electron acceptors with a bulky 3D substituent at the central donor core to minimize non-radiative losses and enhance organic solar cell efficiency, Angew. Chem., Int. Ed. n/a (2024) e202407007, https://doi.org/10.1002/anie.202407007.
[16] S. Guan, Y. Li, C. Xu, N. Yin, C. Xu, C. Wang, M. Wang, Y. Xu, Q. Chen, D. Wang, L. Zuo, H. Chen, Self-assembled interlayer enables high-performance organic

photovoltaics with power conversion efficiency exceeding 20, Adv. Mater. 36 (2024) 2400342, https://doi.org/10.1002/adma.202400342.
[17] Y. Jiang, S. Sun, R. Xu, F. Liu, X. Miao, G. Ran, K. Liu, Y. Yi, W. Zhang, X. Zhu, Non-fullerene acceptor with asymmetric structure and phenyl-substituted alkyl side chain for 20.2% efficiency organic solar cells, Nat. Energy (2024), https://doi.org/10.1038/s41560-024-01557-z.
[18] Y. Sun, L. Wang, C. Guo, J. Xiao, C. Liu, C. Chen, W. Xia, Z. Gan, J. Cheng, J. Zhou, Z. Chen, J. Zhou, D. Liu, T. Wang, W. Li, π-extended nonfullerene acceptor for compressed molecular packing in organic solar cells to achieve over 20% efficiency, J. Am. Chem. Soc. 146 (2024) 12011–12019, https://doi.org/10.1021/jacs.4c01503.
[19] J.-L. Bredas, When electrons leave holes in organic solar cells, Science 343 (2014) 492–493, https://doi.org/10.1126/science.1249230.
[20] Y. Lin, J. Wang, Z.-G. Zhang, H. Bai, Y. Li, D. Zhu, X. Zhan, An electron acceptor challenging fullerenes for efficient polymer solar cells, Adv. Mater. 27 (2015) 1170–1174, https://doi.org/10.1002/adma.201404317.
[21] X. Wan, C. Li, M. Zhang, Y. Chen, Acceptor–donor–acceptor type molecules for high performance organic photovoltaics – chemistry and mechanism, Chem. Soc. Rev. 49 (2020) 2828–2842, https://doi.org/10.1039/D0CS00084A.
[22] J. Yuan, Y. Zhang, L. Zhou, G. Zhang, H.-L. Yip, T.-K. Lau, X. Lu, C. Zhu, H. Peng, P. A. Johnson, M. Leclerc, Y. Cao, J. Ulanski, Y. Li, Y. Zou, Single-junction organic solar cell with over 15% efficiency using fused-ring acceptor with electron-deficient core, Joule 3 (2019) 1140–1151, https://doi.org/10.1016/j.joule.2019.01.004.
[23] G. Zhang, F.R. Lin, F. Qi, T. Heumüller, A. Distler, H.-J. Egelhaaf, N. Li, P.C. Y. Chow, C.J. Brabec, A.K.Y. Jen, H.-L. Yip, Renewed prospects for organic photovoltaics, Chem. Rev. 122 (2022) 14180–14274, https://doi.org/10.1021/acs.chemrev.1c00955.
[24] D. Qian, Z. Zheng, H. Yao, W. Tress, T.R. Hopper, S. Chen, S. Li, J. Liu, S. Chen, J. Zhang, X.-K. Liu, B. Gao, L. Ouyang, Y. Jin, G. Pozina, I.A. Buyanova, W.M. Chen, O. Inganäs, V. Coropceanu, J.-L. Bredas, H. Yan, J. Hou, F. Zhang, A.A. Bakulin, F. Gao, Design rules for minimizing voltage losses in high-efficiency organic solar cells, Nat. Mater. 17 (2018) 703–709, https://doi.org/10.1038/s41563-018-0128-z.
[25] T. Liu, T. Yang, R. Ma, L. Zhan, Z. Luo, G. Zhang, Y. Li, K. Gao, Y. Xiao, J. Yu, X. Zou, H. Sun, M. Zhang, T.A. Dela Peña, Z. Xing, H. Liu, X. Li, G. Li, J. Huang, C. Duan, K.S. Wong, X. Lu, X. Guo, F. Gao, H. Chen, F. Huang, Y. Li, Y. Li, Y. Cao, B. Tang, H. Yan, 16% efficiency all-polymer organic solar cells enabled by a finely tuned morphology via the design of ternary blend, Joule 5 (2021) 914–930, https://doi.org/10.1016/j.joule.2021.02.002.
[26] S. Li, L. Zhan, Y. Jin, G. Zhou, T.-K. Lau, R. Qin, M. Shi, C.-Z. Li, H. Zhu, X. Lu, F. Zhang, H. Chen, Asymmetric electron acceptors for high-efficiency and low-energy-loss organic photovoltaics, Adv. Mater. 32 (2020) 2001160, https://doi.org/10.1002/adma.202001160.
[27] S. Liu, J. Yuan, W. Deng, M. Luo, Y. Xie, Q. Liang, Y. Zou, Z. He, H. Wu, Y. Cao, High-efficiency organic solar cells with low non-radiative recombination loss and low energetic disorder, Nat. Photonics 14 (2020) 300–305, https://doi.org/10.1038/s41566-019-0573-5.
[28] P. Bi, S. Zhang, Z. Chen, Y. Xu, Y. Cui, T. Zhang, J. Ren, J. Qin, L. Hong, X. Hao, J. Hou, Reduced non-radiative charge recombination enables organic photovoltaic cell approaching 19% efficiency, Joule 5 (2021) 2408–2419, https://doi.org/10.1016/j.joule.2021.06.020.
[29] R. Sun, Y. Wu, X. Yang, Y. Gao, Z. Chen, K. Li, J. Qiao, T. Wang, J. Guo, C. Liu, X. Hao, H. Zhu, J. Min, Single-junction organic solar cells with 19.17% efficiency enabled by introducing one asymmetric guest acceptor, Adv. Mater. 34 (2022) 2110147, https://doi.org/10.1002/adma.202110147.
[30] X. Liu, X. Du, J. Wang, C. Duan, X. Tang, T. Heumueller, G. Liu, Y. Li, Z. Wang, J. Wang, F. Liu, N. Li, C.J. Brabec, F. Huang, Y. Cao, Efficient organic solar cells with extremely high open-circuit voltages and low voltage losses by suppressing nonradiative recombination losses, Adv. Energy Mater. 8 (2018) 1801699, https://doi.org/10.1002/aenm.201801699.
[31] Y. Shi, L. Zhu, Y. Yan, M. Xie, G. Liang, J. Qiao, J. Zhang, X. Hao, K. Lu, Z. Wei, Small energetic disorder enables ultralow energy losses in non-fullerene organic solar cells, Adv. Energy Mater. 13 (2023) 2300458, https://doi.org/10.1002/aenm.202300458.
[32] H. Lu, W. Liu, H. Jin, H. Huang, Z. Tang, Z. Bo, High-efficiency organic solar cells with reduced nonradiative voltage loss enabled by a highly emissive narrow bandgap fused ring acceptor, Adv. Funct. Mater. 32 (2022) 2107756, https://doi.org/10.1002/adfm.202107756.
[33] X. Ran, Y. Shi, D. Qiu, J. Zhang, K. Lu, Z. Wei, The central core size effect in quinoxaline-based non-fullerene acceptors for high VOC organic solar cells, Nanoscale 15 (2023) 18291–18299, https://doi.org/10.1039/D3NR05077G.
[34] Z. Zhang, Z. Li, B. Kan, T. Chen, Y. Zhang, P. Wang, Z. Yao, C. Li, B. Zhao, M. Li, T. Duan, X. Wan, Y. Chen, Binary all-polymer solar cells with efficiency over 17% by fine-tuning halogenated thiophene linkers of polymer acceptors, Nano Energy 116 (2023) 108766, https://doi.org/10.1016/j.nanoen.2023.108766.
[35] M. Xie, Y. Shi, L. Zhu, J. Zhang, Q. Cheng, H. Zhang, Y. Yan, M. Zhu, H. Zhou, K. Lu, Z. Wei, Selective halogenation of central and end-units of nonfullerene acceptors enables enhanced molecular packing and photovoltaic performance, Energy Environ. Sci. 16 (2023) 3543–3551, https://doi.org/10.1039/D3EE01333B.
[36] M. Xie, Z. Wei, K. Lu, Quinoxaline-based Y-type acceptors for organic solar cells, Chem. Sci. 15 (2024) 8265–8279, https://doi.org/10.1039/D4SC01481B.
[37] H. Liu, Y. Geng, Z. Xiao, L. Ding, J. Du, A. Tang, E. Zhou, The development of quinoxaline-based electron acceptors for high performance organic solar cells, Adv. Mater. n/a (2024) 2404660, https://doi.org/10.1002/adma.202404660.
[38] X. Si, Y. Huang, W. Shi, R. Wang, K. Ma, Y. Zhang, S. Wu, Z. Yao, C. Li, X. Wan, Y. Chen, Achieving organic solar cells with an efficiency of 18.80% by reducing nonradiative energy loss and tuning active layer morphology, Adv. Funct. Mater. 33 (2023) 2306471, https://doi.org/10.1002/adfm.202306471.
[39] Z. Yao, X. Wan, C. Li, Y. Chen, Two-dimensional conjugation extended CH-series acceptors with a distinctive A–D–A character, Acc. Mater. Res. 4 (2023) 772–785, https://doi.org/10.1021/accountsmr.3c00093.
[40] K. Liu, Y. Jiang, G. Ran, F. Liu, W. Zhang, X. Zhu, 19.7% efficiency binary organic solar cells achieved by selective core fluorination of nonfullerene electron acceptors, Joule 8 (2024) 835–851, https://doi.org/10.1016/j.joule.2024.01.005.
[41] H. Chen, Y. Zou, H. Liang, T. He, X. Xu, Y. Zhang, Z. Ma, J. Wang, M. Zhang, Q. Li, C. Li, G. Long, X. Wan, Z. Yao, Y. Chen, Lowing the energy loss of organic solar cells by molecular packing engineering via multiple molecular conjugation extension, Sci. China Chem. 65 (2022) 1362–1373, https://doi.org/10.1007/s11426-022-1264-y.
[42] Y. Shi, Y. Chang, K. Lu, Z. Chen, J. Zhang, Y. Yan, D. Qiu, Y. Liu, M.A. Adil, W. Ma, X. Hao, L. Zhu, Z. Wei, Small reorganization energy acceptors enable low energy losses in non-fullerene organic solar cells, Nat. Commun. 13 (2022) 3256, https://doi.org/10.1038/s41467-022-30927-y.
[43] H. Liang, X. Bi, H. Chen, T. He, Y. Lin, Y. Zhang, K. Ma, W. Feng, Z. Ma, G. Long, C. Li, B. Kan, H. Zhang, O.A. Rakitin, X. Wan, Z. Yao, Y. Chen, A rare case of brominated small molecule acceptors for high-efficiency organic solar cells, Nat. Commun. 14 (2023) 4707, https://doi.org/10.1038/s41467-023-40423-6.
[44] K. Liu, Y. Jiang, F. Liu, X. Zhu, Quinoxaline-based nonfullerene acceptors with powerful core-functionalization ability enabling efficient solar energy utilization, Energy Environ. Sci. (2024), https://doi.org/10.1039/D4EE01474J.
[45] X. Bi, X. Cao, T. He, H. Liang, Z. Yao, J. Yang, Y. Guo, G. Long, B. Kan, C. Li, X. Wan, Y. Chen, What is the limit size of 2D conjugated extension on central units of small molecular acceptors in organic solar cells? Small (2024) 2401054 https://doi.org/10.1002/smll.202401054.
[46] J. Liu, H. Zhang, H. Dong, L. Meng, L. Jiang, L. Jiang, Y. Wang, J. Yu, Y. Sun, W. Hu, A.J. Heeger, High mobility emissive organic semiconductor, Nat. Commun. 6 (2015) 10032, https://doi.org/10.1038/ncomms10032.
[47] Y. Cui, P. Zhu, H. Hu, X. Xia, X. Lu, S. Yu, H. Tempeld, R.-A. Eichel, X. Liao, Y. Chen, Impact of Electrostatic Interaction on Non-radiative Recombination, Energy Losses Org. Sol. Cells Based Asymmet Accept. Angew. Chem. Int. Ed. 62 (2023) e202304931, https://doi.org/10.1002/anie.202304931.
[48] N. Niharika Bhuyan, S. Shankar S, S. Jyoti Panda, C. Shekhar Purohit, R. Singhal, G.D. Sharma, A. Mishra, An asymmetric coumarin-anthracene conjugate as efficient fullerene-free acceptor for organic solar cells, Angew. Chem. Int. Ed. n/a (2024) e202406272, https://doi.org/10.1002/anie.202406272.
[49] Z. Shuai, H. Geng, W. Xu, Y. Liao, J.-M. André, From charge transport parameters to charge mobility in organic semiconductors through multiscale simulation, Chem. Soc. Rev. 43 (2014) 2662–2679, https://doi.org/10.1039/C3CS60319A.
[50] X.-K. Chen, D. Qian, Y. Wang, T. Kirchartz, W. Tress, H. Yao, J. Yuan, M. Hülsbeck, M. Zhang, Y. Zou, Y. Sun, Y. Li, J. Hou, O. Inganäs, V. Coropceanu, J.-L. Bredas, F. Gao, A unified description of non-radiative voltage losses in organic solar cells, Nat. Energy 6 (2021) 799–806, https://doi.org/10.1038/s41560-021-00843-4.
[51] N.J. Hestand, F.C. Spano, Expanded theory of H- and J-molecular aggregates: the effects of vibronic coupling and intermolecular charge transfer, Chem. Rev. 118 (2018) 7069–7163, https://doi.org/10.1021/acs.chemrev.7b00581.
[52] Y. Zeng, D. Li, Z. Xiao, H. Wu, Z. Chen, T. Hao, S. Xiong, Z. Ma, H. Zhu, L. Ding, Q. Bao, Exploring the charge dynamics and energy loss in ternary organic solar cells with a fill factor exceeding 80, Adv. Energy Mater. 11 (2021) 2101338, https://doi.org/10.1002/aenm.202101338.
[53] R. Wang, C. Zhang, Q. Li, Z. Zhang, X. Wang, M. Xiao, Charge separation from an intra-moiety intermediate state in the high-performance PM6:Y6 organic photovoltaic blend, J. Am. Chem. Soc. 142 (2020) 12751–12759, https://doi.org/10.1021/jacs.0c04890.
[54] F. Liu, Y. Jiang, R. Xu, W. Su, S. Wang, Y. Zhang, K. Liu, S. Xu, W. Zhang, Y. Yi, W. Ma, X. Zhu, Nonfullerene acceptor featuring unique self-regulation effect for organic solar cells with 19% efficiency, Angew. Chem., Int. Ed. 63 (2024) e202313791, https://doi.org/10.1002/anie.202313791.
[55] J. Song, C. Zhang, C. Li, J. Qiao, J. Yu, J. Gao, X. Wang, X. Hao, Z. Tang, G. Lu, R. Yang, H. Yan, Y. Sun, Non-halogenated solvent-processed organic solar cells with approaching 20% efficiency and improved photostability, Angew. Chem. Int. Ed. 63 (2024) e202404297, https://doi.org/10.1002/anie.202404297.